ELSEVIER

International Journal of Mass Spectrometry 197 (2000) 113–121

International Journal of Mass Spectrometry

Peak structure with a quadrupole mass filter operated in the third stability region

Zhaohui Du[a], D.J. Douglas[a], Tatyana Glebova[b], N.V. Konenkov[b,*]

[a]*Department of Chemistry, University of British Columbia, 2036 Main Mall, Vancouver, British Columbia V6T 1Z1, Canada*
[b]*Department of General Physics, Ryazan State Pedagogical University, Svoboda Strasse 46, 390000, Ryazan, Russia*

Received 23 August 1999; accepted 22 September 1999

Abstract

Peak structure for a quadrupole operated in the third stability region with Mathieu parameters (a, q) ≈ (3, 3) has been studied experimentally and modeled theoretically. It is shown that the structure is due to the imaging properties of the quadrupole field which are caused by the wavelike properties of the ion trajectories. Ions enter the quadrupole through a small inlet aperture on axis. When ions are focused on the center of the exit aperture the transmission is a maximum. Conversely when ions have trajectories that place them near the rods at the exit aperture the transmission is a minimum and a dip appears on a peak. The positions of dips on a peak can be assigned to lines in the stability diagram. These lines follow iso-β lines, where β is the parameter that determines the frequencies of ion motion. The positions of the lines are controlled by the number of rf cycles, which ions spend in the quadrupole field. At high resolution (>300) and low ion axial energy (<20 eV) the peak splitting is minimal or absent. (Int J Mass Spectrom 197 (2000) 113–121) © 2000 Elsevier Science B.V.

Keywords: Quadrupole mass filter; Third stability region; Peak shape; Peak structure; Frequencies

1. Introduction

Ion motion in a quadrupole mass filter is determined by the two Mathieu parameters a and q given by

$$a = \frac{8eU}{m_{\text{ion}}\omega^2 r_0^2}, \qquad q = \frac{4eV}{m_{\text{ion}}\omega^2 r_0^2} \tag{1}$$

where e is the charge on an ion, m_{ion} is the ion mass, ω is the angular frequency of the rf voltage applied to the quadrupole, r_0 is the distance from the center of the quadrupole to an electrode ("the field radius"), U is the dc voltage applied from pole to ground, and V is the zero to peak rf voltage applied from pole to ground. Combinations of a and q which give ion motion that is stable in the x and y directions, orthogonal to the quadrupole axis, form "stability regions."

The "third" stability region is a nonlinear quadrangle, located near $a = 3$ and $q = 3$ [1–4]. This region is of interest, particularly for atomic mass spectrometry [3,5], because it has reasonably high transmission and a resolution of several thousand can be obtained at low m/e [3–6]. The third stability region has two working regions, an upper tip "M," and a lower tip "S." These are shown in detail in Figs. 1 and 2. The dashed lines are iso-β lines where β is the stability

* Corresponding author. E-mail: konenkov@ttc.ryazan.ru

PII S1387-3806(99)00222-5

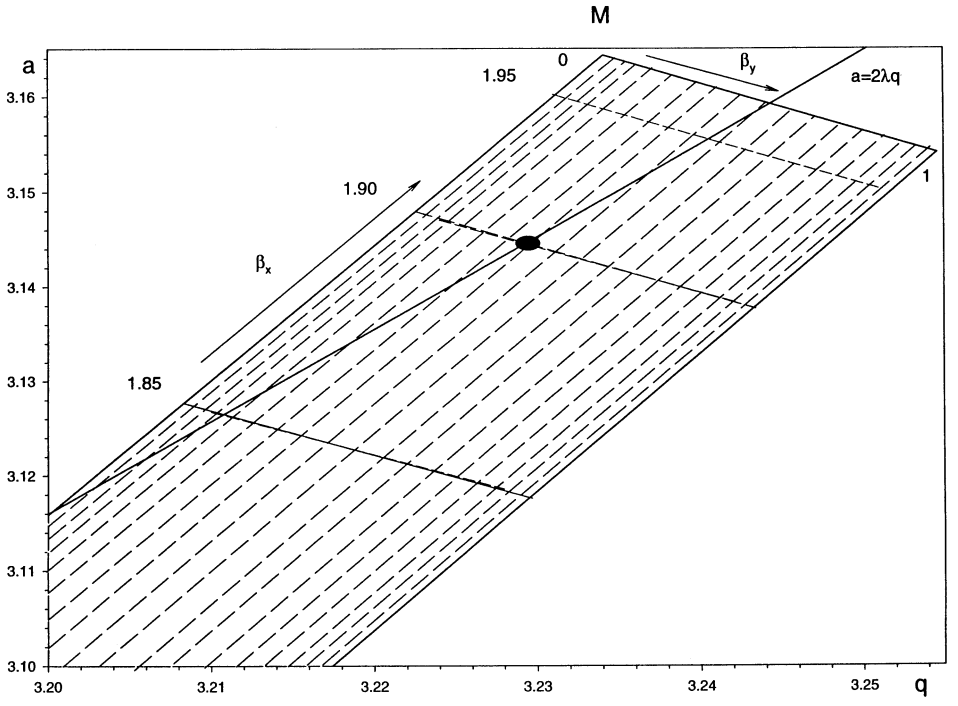

Fig. 1. The third stability region near the upper tip M. The iso-β lines correspond to the lines giving maxima for $n = 20$. The β_y lines are from 0.1 to 0.9 in steps of 0.05.

parameter and $0 < \beta_y < 1$ and $1 < \beta_x < 2$. The iso-β_y lines in Fig. 1 have β values from 0.1 to 0.9 with steps of 0.05. The boundaries of the third stability zone where y motion becomes unstable correspond to $\beta_y = 0$ and $\beta_y = 1$ and the boundaries where x motion becomes unstable correspond to $\beta_x = 1$ and $\beta_x = 2$. (For positive ions, the x direction is the direction of the poles with the positive dc voltage.)

We have observed that with operation of a quadrupole with relatively high ion energy (50–100 eV) in the third and other higher stability regions, peaks often show structure with a series of dips. This is discussed for the second stability region [$(a, q) = (0.02, 7.55)$] in [7]. This article discusses structure with quadrupole operation in the third region. We calculate from quadrupole theory the positions of the dips expected on a peak from ion collection effects. Ions enter the quadrupole through a small aperture on axis. When ions are focused to the center of the quadrupole at the exit in either the x or y direction, the ion transmission is a maximum. Conversely, when ions are near the rods at the quadrupole exit the transmission is a minimum. In the higher stability regions the fringing fields are more strongly defocusing than in the first region. To overcome this, higher ion energies are often used and as we discuss in Sec. 5, this leads to more pronounced ion collection effects. Positions on the peak where a dip is formed lie on lines in the stability region. Comparisons of the calculations to experimental peak shapes show that the imaging properties of the quadrupole field [8] are responsible for the peak splitting. The same imaging phenomena are the basis for the operation of a focussing monopole [9].

2. Experiment

Peak shapes were recorded with the apparatus described previously [5]. Briefly, an inductively cou-

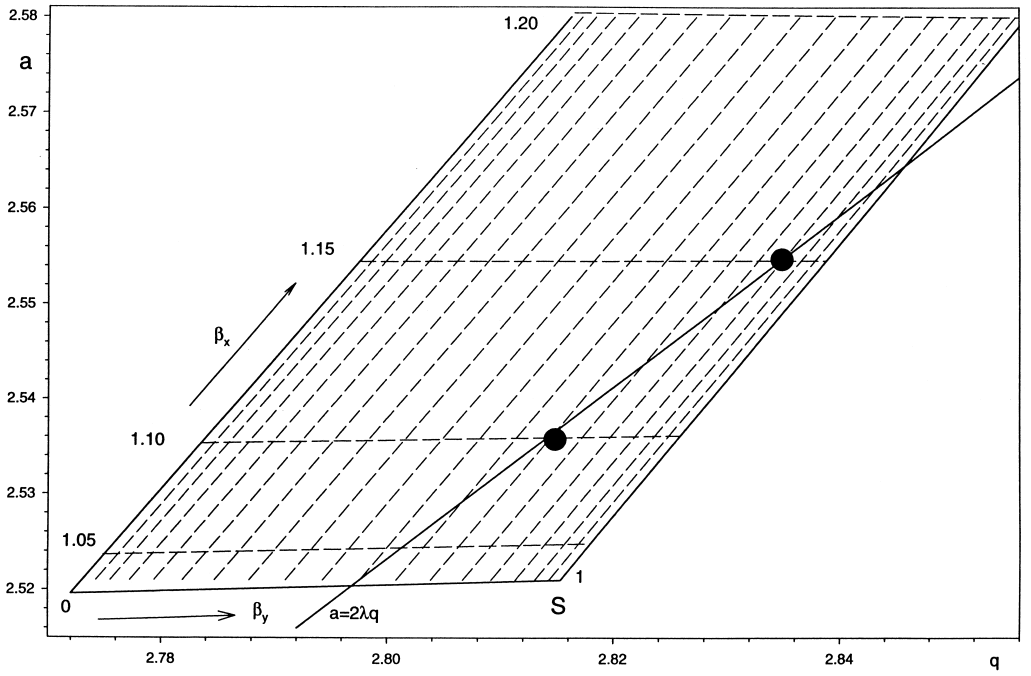

Fig. 2. The third stability region near the lower tip S. The iso-β lines correspond to the lines giving maxima for $n = 20$. The β_y lines are from 0.1 to 0.9 in steps of 0.05. The solid circles are points where ions are focused at the exit aperture in both the x and y directions.

pled plasma produced ions that were sampled through a three-aperture differentially pumped interface. Ions pass through a series of cylindrical lenses and then an aperture plate at the entrance to the quadrupole (aperture diameter 1.33 mm). The aperture plate was held at −177 V. The mass filter rods were 21.2 cm long and 15.9 mm diameter. The nominal ratio of rod radius (r) to field radius (r_0) was $r/r_0 = 1.128$ and the rf frequency was 1.20 MHz. An ion optical schematic of the QMF is shown in Fig. 3. The output aperture diameter was 15 mm. Ions were detected with a channel electron multiplier (Galileo, Sturbridge MA, model 4879) mounted off axis with the detector entrance between the x and y rods. The entrance to the multiplier was operated at a potential of about −4500 V.

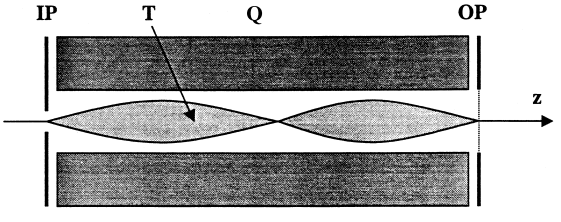

Fig. 3. Ion optical schematic of the quadrupole rod set. IP is the input plate with orifice diameter 1.33 mm, OP is output plate with orifice diameter 15 mm, Q is the quadrupole and T are ion trajectories with $\lambda = L$.

For these experiments the transport (axial) energy of $^{59}Co^+$ ions in the quadrupole could be varied from an initial kinetic energy of about 3 eV (the ion energy from the source) to 120 eV by changing the rod offset voltage of the quadrupole. Ion counting was used for detection. Peaks were recorded with a step size of 0.01 m/z and typically ten scans were averaged to produce a spectrum.

3. Fundamental frequencies of ion oscillation

To calculate the focusing properties of a quadrupole mass filter it is necessary to know the fundamental frequencies of ion motion in the x and y directions

[7–9]. The ion motion in any stability region in the x (or y) direction is described by [1]

$$x(\xi) = A \sum C_{2n} \sin [(2n + \beta_x)\xi] + B \sum C_{2n} \cos [(2n + \beta_x)\xi] \quad (2)$$

where A and B are constants depending on the initial conditions, $\xi = \omega t/2$ is proportional to the time t, $n = 0, \pm 1, \pm 2, \pm 3, \ldots$ and C_{2n} are terms of the expansion which depend on the (a, q) point in the stability region. From Eq. (2) it follows that the frequencies of ion oscillation, Ω, can be written as

$$\Omega_n = (2n + \beta)\omega/2, \qquad n = 0, \pm 1, \pm 2, \pm 3, \ldots \quad (3)$$

The frequencies of ion motion are independent of the initial rf phase when the ions enter the quadrupole field [1]. In theory, ion collection effects can be formed at any frequency Ω_n. However a comparison of theory and experiment for the second stability region [7] shows that collection effects are observed only on the lowest frequencies of ion oscillation. From Eq. (3), the fundamental frequencies for stability zones with $\beta > 1$ are not immediately apparent. This is because of the beatlike nature of ion motion caused by interferences between frequencies with different values of n in Eq. (3).

If the parameter β is represented by a rational ratio

$$\beta = m + P/S \quad (4)$$

where $m = 0, 1, 2, 3, \ldots$ are Mathieu function indices of integer order, P and S are simple integers and $P < S$, then the ion motion described by Eq. (2) will be periodic with period $2\pi S$ [9,10]. Near the stability boundary, ion oscillations appear as beats. For the third stability region this is confirmed here by numerical trajectory calculations (Fig. 4). Hence, for example, near the upper tip of the third stability region (Fig. 1) $\beta_x \to 2$, $m = 1$ and $P/S \approx 1$, $\beta_y \to 0$, $m = 0$ and $P/S \ll 1$. For these conditions according to [9] we can write

$$\beta_x = 1 + (S - 1)/S, \qquad \beta_y = 1/S \quad (5)$$

where S is a large integer number. As $\xi = \omega t/2$ then $2\pi S = 2\pi\omega/2\Omega$ and the fundamental frequency of ion oscillation in y is given by

$$\Omega_y = \omega/2S \quad (6)$$

Expressing S from Eq. (4) and substituting it in Eq. (5) we find that the fundamental frequencies Ω_x and Ω_y of ion oscillations in the xz and yz planes with operation at the upper tip are given by

$$\Omega_x = (2 - \beta_x)\omega/2 \qquad \text{for } 1.5 \le \beta_x < 2 \quad (7)$$

$$\Omega_y = \beta_y\omega/2 \qquad \text{for } 0 < \beta_y \le 0.5 \quad (8)$$

In the same way for the lower tip the fundamental frequencies of ion oscillation are given by

$$\Omega_x = (\beta_x - 1)\omega/2 \qquad \text{for } 1 < \beta_x \le 1.5 \quad (9)$$

$$\Omega_y = (1 - \beta_y)\omega/2 \qquad \text{for } 0.5 \le \beta_y < 1 \quad (10)$$

To verify the relations (7)–(10) the ion trajectories for four cases were calculated. The ion trajectories in the xz and yz planes of the mass filter are shown in Fig. 4. The ion oscillations have the appearance of beats with the fundamental frequency Ω.

From Fig. 4(a) with $\beta_x = 1.81$ we have $T_\Omega/T_\omega \cong 2(26 - 9)/\pi \approx 10.8$, where $T_\Omega = 2\pi/\Omega_x$ and $T_\omega = 2\pi/\omega$. (The time axis in Fig. 4 is in the variable ξ. Because $\xi = \omega t/2$, the period T_ω for one rf cycle corresponds to the value π for the variable ξ.) From Eq. (7) we find that $\omega/\Omega_x = 2/(2 - \beta_x) \approx 10.6$. From the data of Fig. 4(b) for $\beta_x \cong 1.11$ it can be estimated that $T_\Omega/T_\omega \cong 2(41 - 13)/\pi \approx 17.8$. From Eq. (9) $\omega/\Omega_x = 2/(\beta_x - 1) \approx 17.6$. Analogously, from Fig. 4(c) ($\beta_y \cong 0.24$) we find that $T_\Omega/T_\omega \cong (40 - 14)/\pi \approx 8.3$. From Eq. (8) the ratio $\omega/\Omega_y = 2/\beta_y \approx 8.3$. From Fig. 4(d) and from Eq. (10) we find that $T_\Omega/T_\omega = \omega/\Omega_y \approx 20$. Thus the numerical ion trajectory simulations demonstrate the validity of relations (7)–(10).

4. Conditions for ion detection effects

The trajectories of Fig. 4 show that the ion motion has a wavelike character. If the ion motion happens to

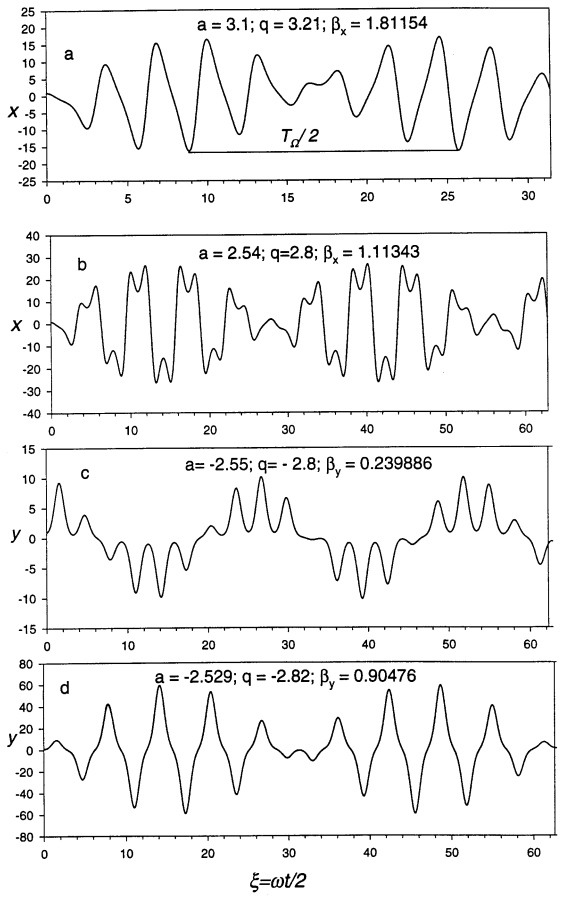

Fig. 4. Ion trajectories at different points (a, q) in the third stability region: (a) $a_x = 3.1$, $q_x = 3.21$ ($\beta_x = 1.811\,54$); (b) $a_x = 2.54$, $q_x = 2.8$ ($\beta_x = 1.113\,43$); (c) $a_y = -2.55$, $q_y = -2.8$ ($\beta_y = 0.239\,88$); (d) $a_y = -2.529$, $q_y = -2.82$ ($\beta_y = 0.904\,76$). Initial positions are 1.0 which corresponds to $0.001\ r_0$ (i.e. the vertical axis is in units of $10^{-3}\ r_0$). Initial radial velocities are zero.

lead to the ions reaching the exit aperture on the center line, the ion transmission will be a maximum. If the ions reach the exit near the rods, the fringing fields can defocus the ions and decrease the transmission to the detector, leading to a dip on a peak. Ions will be at the center of the exit aperture when the quadrupole length L is an integer number, k, of half wavelengths $\lambda/2$. That is when

$$(\lambda/2)k = L, \qquad k = 1, 2, 3, \ldots \tag{11}$$

where $\lambda = v_z T_\Omega$ is the wavelength, v_z is the axial ion velocity, and T_Ω is the period of ion fundamental oscillation with frequencies Ω_x and Ω_y in the x and y directions. This is shown schematically in Fig. 3 where $L = 2(\lambda/2)$. In this case the ion beam is focused on the center of the output aperture and the output ion current is a maximum. The periodicity condition is $x(\xi_0 + 2\pi Q) = x(\xi_0)$ for all initial phases. This means the entrance aperture of diameter d is focused on the exit with a beam diameter d, regardless of the rf phase.

With maximum amplitudes of ion oscillation at the quadrupole output, ions will be deflected by the fringing fields, not all ions will be detected, and there will be a minimum in the ion current. In these cases the peak will have dips and will be distorted (e.g. Fig. 5). The appearance of a dip (a local minimum of ion current) corresponds to the condition that the quadrupole length L is an odd integer number, $2k + 1$, of quarter wavelengths $\lambda/4$

$$(\lambda/4)(2k + 1) = L, \qquad k = 0, 1, 2, 3, \ldots \tag{12}$$

From expressions (7)–(10) we can write the periods T_x and T_y of the fundamental ion oscillations at the upper tip M (Fig. 1) and lower tip S (Fig. 2) of the third stability region as

$$T_x = 2\pi/\Omega_x = 2/\Delta_x f, \tag{13a}$$

where

$$\Delta_x = 2 - \beta_x, \qquad 1.5 \leq \beta_x < 2\ (\mathrm{M}) \tag{13b}$$

$$\Delta_x = \beta_x - 1, \qquad 1 < \beta_x \leq 1.5\ (\mathrm{S}) \tag{13c}$$

and

$$T_y = 2\pi/\Omega_y = 2/\Delta_y f \tag{14a}$$

$$\Delta_y = \beta_y, \qquad 0 < \beta_y \leq 0.5\ (\mathrm{M, S}) \tag{14b}$$

$$\Delta_y = 1 - \beta_y, \qquad 0.5 < \beta_y \leq 1.0\ (\mathrm{S, M}) \tag{14c}$$

Conditions (11) and (12) for maxima and minima of ion signals can be written in the form

$$k = \Delta_x n \text{ and/or}$$

$$j = \Delta_y n; \qquad (15)$$

$$k, j = 1, 2, 3, \ldots \quad \text{(max)}$$

$$2k + 1 = \Delta_x 2n \text{ and/or}$$

$$2j + 1 = \Delta_y 2n; \qquad (16)$$

$$k, j = 0, 1, 2, 3, \ldots \quad \text{(min)}$$

where $n = L/v_z T = Lf/v_z$ is the number of rf cycles which ions spend in the quadrupole field. For tips M and S Eq. (15) determines the lines in the stability diagram for maximum signal in terms of the parameters β_x and β_y as

$$\text{M: } \beta_x = 2 - (k/n), \qquad 1.5 \leq \beta_x < 2 \qquad (17)$$

$$\text{S: } \beta_x = 1 + (k/n), \qquad 1 < \beta_x \leq 1.5 \qquad (18)$$

$$\text{(M, S): } \beta_y = k/n, \qquad 0 < \beta_y \leq 0.5 \qquad (19)$$

$$\text{(M, S): } \beta_y = 1 - (k/n), \qquad 0.5 \leq \beta_y < 1 \qquad (20)$$

where $k = 1, 2, 3, \ldots$. The iso-β lines which correspond to dips (minima) can be determined from Eq. (16). For the M and S tips the conditions for observing dips on a peak are

$$\text{M: } \beta_x = 2 - (2k + 1)/2n, \qquad 1.5 \leq \beta_x < 2 \qquad (21)$$

$$\text{S: } \beta_x = 1 + (2k + 1)/2n, \qquad 1 < \beta_x \leq 1.5 \qquad (22)$$

$$\text{(M, S): } \beta_y = (2k + 1)/2n, \qquad 0 < \beta_y \leq 0.5 \qquad (23)$$

$$\text{(M, S): } \beta_y = 1 - (2k + 1)/2n, \qquad 0.5 \leq \beta_y < 1 \qquad (24)$$

where $k = 0, 1, 2, 3, \ldots$. The lines for maximum signal are shown in Figs. 1 and 2 for a typical case, $n = 20$.

5. Peak structure and identification

Peak-shape distortions and peak splitting for $^{59}Co^+$ ions with a quadrupole operated in the third stability region at the upper tip M (~63 eV ion energy) are illustrated in Fig. 5(a) and at the lower tip S (~53 eV ion energy) in Fig. 5(b). The peak shape distortions are found to be worse at higher ion energies. At low energies there are more dips, more narrowly separated, and the energy spread from the source tends to "wash out" the structure [7]. In our system the structure is much more pronounced at ion energies of 50–100 eV than at a few electron volts.

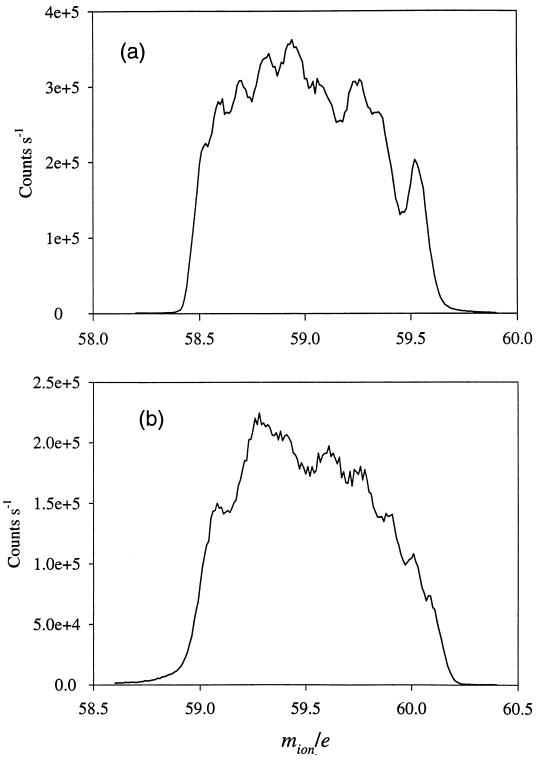

Fig. 5. Peak shape of $^{59}Co^+$ ions at (a) the M tip, resolution $R = 48$, 63 eV ion energy and (b) the S tip, $R = 43$, 53 eV ion energy.

An observed dip on the peak can be assigned to a line in the stability diagram which is determined by Eqs. (21)–(24) as follows. At different values of the resolution R, corresponding to the different scan lines $a = 2\lambda q$ shown in Fig. 6(a), the peak was displayed as in Fig. 5. The resolution $R = m/\Delta m$ obtained for the peak was determined by means of directly measuring the mass width at a level close to zero. From this value of R, the value of $\lambda = U/V$ of the scan line $a = 2\lambda q$ was calculated using the straight line approximations to the boundaries of the stability region (Fig. 2). The value of λ at S is given by

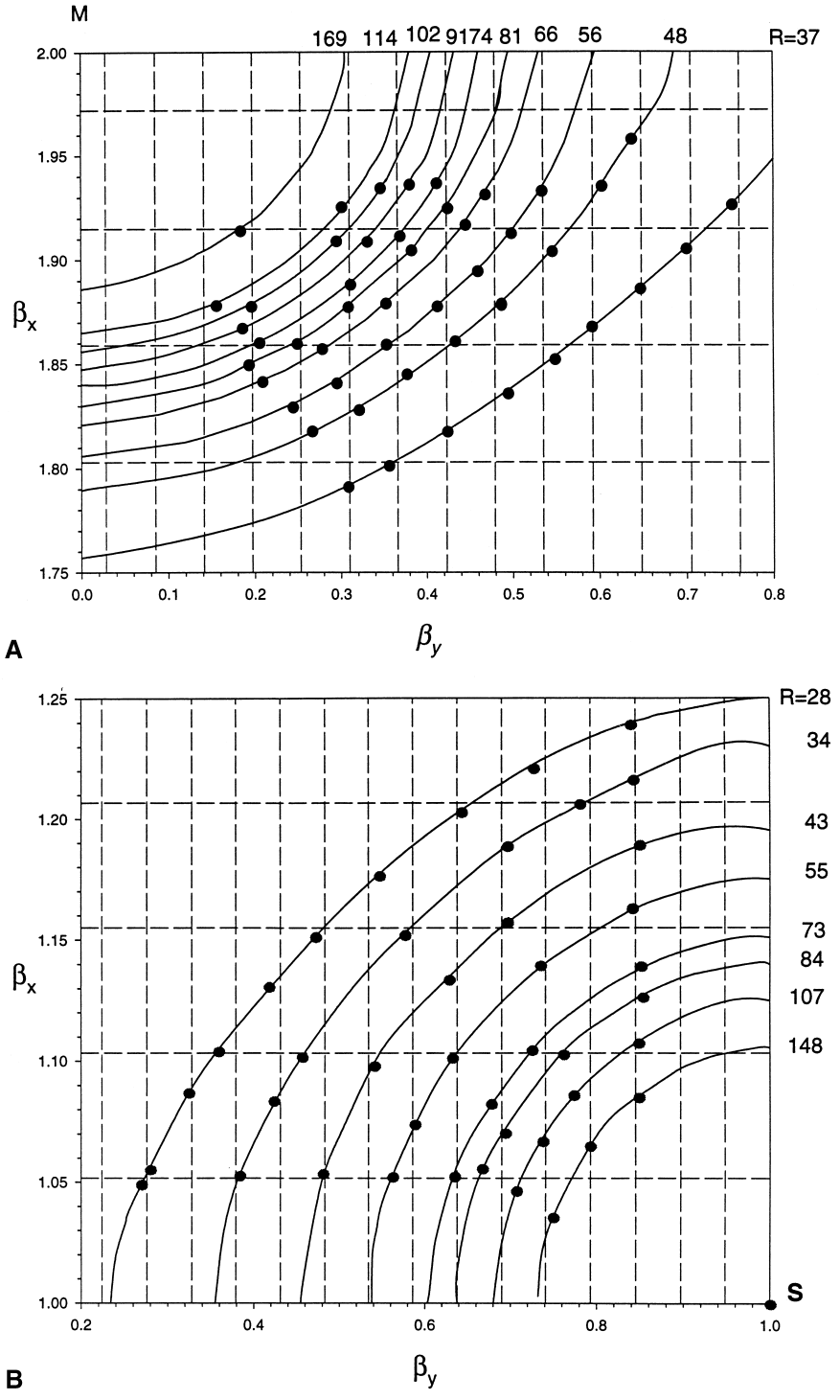

Fig. 6. Scan lines at tips M (a) and (S) (b) in β_x and β_y variables for different resolutions (solid lines). Dashed lines correspond to detection minima (A) and maxima (B) lines. Solid points are the experimental positions of minima (A) and maxima (B).

$$\lambda = [(R - 0.5)3.499\ 73 + 3.4475]/[4.8442 + (R - 0.5)7.816\ 56] \quad (25)$$

and at M by

$$\lambda = [(R - 0.5)5.987\ 79 - 0.670\ 165]/[(R - 0.5)12.239\ 67 + 2.699\ 07] \quad (26)$$

Thus for example $R = 48$ ($\lambda = 0.4858$) for the peak of Fig. 5(a) and $R = 43$ ($\lambda = 0.451\ 53$) for the peak of Fig. 5(b). The scan lines $a = 2\lambda q$ are then plotted on the stability diagrams in β_x and β_y variables [Fig. 6(a) and 6(b)]. The points corresponding to minima (or maxima) on a peak are plotted and compared to the previously calculated iso-β lines for a minimum (or maximum), shown by the dashed lines in Fig. 6. As a result we are able to determine the line which corresponds to a particular dip on the mass peak. This is illustrated in Fig. 6(a) and 6(b). The positions of the observed dips for different resolutions R are shown in Fig. 6(a) for an ion energy $E_z = 63$ eV (3 eV is initial kinetic ion energy from ion source plus eU_z, where $U_z = -60$ V is the rod offset voltage). The positions of the observed local maxima on the peak are shown in Fig. 6(b) for operation at the lower tip S with an ion energy $E_z = 53$ eV. According to Eqs. (17)–(20) a minimum corresponds to the scan line $a = 2\lambda q$ crossing the iso-β_x or iso-β_y lines. When the scan line crosses the iso-β_x and iso-β_y lines simultaneously the dip or maximum is stronger because ion defocussing takes place in both the x and y directions. Examples of this are shown in Fig. 2. From conditions (17)–(24) it is follows that the distance between lines is $\Delta\beta_x = \Delta\beta_y = 1/n$. For the experimental conditions $L = 21.2$ cm, $r_0 = 6.195$ mm, and $f = 1.2$ MHz and for a given acceleration voltage U_z the number of rf cycles, n, which ions experience in the quadrupole field, is given by

$$n = Lf\sqrt{\frac{M}{2eN_AU_z}} = \frac{140.766}{\sqrt{E_z}} \quad (27)$$

where $M = 59$ u, $e = 1.602 \times 10^{-19}$ C, $N_A = 6.022 \times 10^{26}$ kmol^{-1}, and E_z is the axial ion energy expressed in electron volts. From Eq. (27) we have $n = 17.74$ for an ion energy $E_z = 63$ eV [Fig. 6(a)] and $\Delta\beta = 1/n = 0.0564$ and for an ion energy 53 eV [Fig. 6(b)] $n = 19.34$ and $\Delta\beta = 0.0517$. The calculated lines for minima correspond to $\beta_x = 2 - (2k + 1)(0.028)$ and $\beta_y = (2k + 1)(0.028)$ ($k = 0, 1, 2, \ldots$). These are shown by the dashed lines in Fig. 6(a) for the upper tip M. The positions of maxima on the peak are illustrated in Fig. 6(b) for the lower tip S. These follow approximately the iso-β lines: $\beta_x = 1 + k(0.0517)$ and $\beta_y = 1 - k(0.0517)$, where $k = 1, 2, \ldots$.

In Fig. 6 solid points, which represent observed maxima and minima, are located near the calculated iso-β lines. The average distance $\Delta\beta$ between them approximately equals $1/n$ in accord with the theoretical predictions (17)–(24). It is also observed that the positions of dips on a peak change with changing axial ion energy. This confirms the proposed mechanism for the observed peak splitting. In principle nonlinear resonances [1,11,12] can cause peak splitting and these may also follow iso-β lines. However with nonlinear resonances the positions of dips do not change with ion energy. Also nonlinear resonances are expected to be more severe at low ion energies where the resonances have more time to build up. The peak structure we observe is more pronounced at high ion energies.

The dip positions may be changed by an inbalance in the voltages applied to opposite pairs of rods, a shift of the input orifice from center and details of the ion detector mounting (on axis, off axis in x or y etc). The intensity of the dips (Fig. 5) is controlled by the size of input orifice (Fig. 3) and the axial ion energy E_z. At low ion energy (for our experimental conditions less than about 20 eV) the difference $\Delta\beta = 1/n$ is small, the ion energy spread gives a spread in n, and the structure is lost. A smooth peak is formed. At high resolution (>300) the dips are weak or absent because the lines do not pass through the working region at the tip of the stability region at ion energy $E_z > 60$ eV.

6. Conclusions

With quadrupole operation in the third stability region, ion collection effects dominate over nonlinear resonances, at least for the conditions of our experiment. The observed peak splitting derives from the wavelike ion motion when ions spend a low number of rf cycles in the quadrupole field. Removing this undesirable peak splitting will require changes to the ion inlet optics or changes to the ion detection geometry.

Acknowledgements

This work was supported through an NSERC-SCIEX Industrial Chair. Travel by one of the authors (N.V.K.) to the University of British Columbia was supported by the "Going Global" program of the Canadian Association of University Teachers.

References

[1] Quadrupole Mass Spectrometry and Its Applications, P.H. Dawson (Ed.), Elsevier, Amsterdam, 1976, reissued by AIP, Woodbury, New York, 1995.
[2] P.H. Dawson, J. Vac. Sci. Technol. 11 (1974) 1151.
[3] Z. Du, D.J. Douglas, N.V. Konenkov, J. Anal. At. Spectrom. 14 (1999) 1111.
[4] N.V. Konenkov, V.I. Kratenko, Int. J. Mass Spectrom. Ion Processes 108 (1991) 115.
[5] Z. Du, T.N. Olney, D.J. Douglas, J. Am. Soc. Mass Spectrom. 8 (1997) 1230.
[6] R.E. Pedder, R.A. Schaeffer, presented at the 43rd and 44th ASMS Conferences on Mass Spectrometry and Allied Topics; Atlanta, Georgia, 21–26 May 1995 and Portland, OR, 12–16 May 1996, respectively.
[7] Z. Du, D.J. Douglas, N.V. Konenkov, J. Am. Soc. Mass Spectrom., in press.
[8] P.H. Dawson, Adv. Electron. Electron Phys. 53 (1980) 153.
[9] R.F. Lever, IBM J. Res. Dev. 10 (1966) 26.
[10] M. Abramowitz, I. Stegun, Handbook of Mathematical Functions, Applied Mathematical Series Vol. 55, National Bureau of Standards, Washington, DC, 1964, p. 537.
[11] Y. Wang, J. Franzen, K.P. Wanczek, Int. J. Mass Spectrom. Ion Processes 124 (1993) 125.
[12] Y. Wang, J. Franzen, Int. J. Mass Spectrom. Ion Processes 132 (1994) 155.